Real-time processing for full-range Fourier-domain optical-coherence tomography with zero-filling interpolation using multiple graphic processing units

Yuuki Watanabe,* Seiya Maeno, Kenji Aoshima, Haruyuki Hasegawa, and Hitoshi Koseki

Graduate School of Science and Engineering, Yamagata University, 4-3-16 Johnan, Yonezawa, Yamagata 992-8510, Japan

*Corresponding author: ywata@yz.yamagata-u.ac.jp

Received 13 April 2010; revised 20 July 2010; accepted 25 July 2010; posted 26 July 2010 (Doc. ID 126883); published 26 August 2010

The real-time display of full-range, 2048 axial pixel × 1024 lateral pixel, Fourier-domain optical-coherence tomography (FD-OCT) images is demonstrated. The required speed was achieved by using dual graphic processing units (GPUs) with many stream processors to realize highly parallel processing. We used a zero-filling technique, including a forward Fourier transform, a zero padding to increase the axial data-array size to 8192, an inverse-Fourier transform back to the spectral domain, a linear interpolation from wavelength to wavenumber, a lateral Hilbert transform to obtain the complex spectrum, a Fourier transform to obtain the axial profiles, and a log scaling. The data-transfer time of the frame grabber was 15.73 ms, and the processing time, which includes the data transfer between the GPU memory and the host computer, was 14.75 ms, for a total time shorter than the 36.70 ms frame-interval time using a line-scan CCD camera operated at 27.9 kHz. That is, our OCT system achieved a processed-image display rate of 27.23 frames/s.

OCIS codes: 100.2000, 110.4500, 170.4500.

1. Introduction

Optical-coherence tomography (OCT) is an interferometric imaging technique that provides high-resolution, cross-sectional imaging of biological tissue [1]. Conventional time-domain (TD) OCT detects echo time delays of backreflected and backscattered light by measuring the interference signal as a function of time during a depth A-scan along each position of a lateral probe beam in a reference arm. In Fourier-domain (FD) OCT, depth information can be retrieved by detecting the interference signal as a function of wavelength instead of with a mechanical A-scan. Spectral-domain (SD) OCT is achieved with a broadband source and a spectrometer on a detector arm [2,3]. Swept source OCT uses a wavelength-scanning laser and a point detector to acquire the same information [4,5].

The main advantage of FD-OCT over TD-OCT is a marked increase in sensitivity [6]. Hence, OCT images of biological tissue can be obtained with a sufficient signal-to-noise ratio (SNR) at an increased imaging speed. Spectrometers with linear-array detectors and swept sources normally operate at tens of kHz, allowing video-rate data acquisition [30 frames/s (fps)]. More recently, ultrahigh-speed FD-OCT techniques have been demonstrated using an FD mode-locked laser at sweep rates of 370 kHz [7] and a complementary metal-oxide semiconductor (CMOS) line-scan camera at 312.5 kHz [8].

FD-OCT images require resampling of the axial data from wavelength (λ)-space to wavenumber

0003-6935/10/254756-07$15.00/0

($k = 2\pi/\lambda$)-space, and the subsequent application of the inverse Fourier transform. The simplest resampling procedure is to perform a linear interpolation, but it leads to errors at greater depths because of the increased background or shoulders around the peaks; these, however, can be addressed with a zero-filling technique [9–11]. This correction involved a forward Fourier transform, zero padding to increase the data-array length M-fold, and an inverse Fourier transform back to the spectral data. The common values used for M were 4 and 8. This spectral data, which was M times larger than the original array, is linearly interpolated to k-space and Fourier transformed into z-space to obtain depth information. Therefore, the calculation time for this technique is considerably longer than that for the simple linear interpolation.

The standard FD-OCT image contains DC and conjugate artifacts, and suffers from a strong SNR falloff, which is proportional to the distance from zero-delay. In general, DC components (i.e., fixed-pattern noise) can be removed by subtracting the reference beam intensity. The sample must be carefully located below the zero-delay line to avoid overlapping the real image and its conjugate mirror image. However, because the system sensitivity is highest around the zero-delay, advantages exist to imaging with the zero-delay inside the sample.

One of the aims of achieving full-range FD-OCT without artifacts was accomplished by using a spatial phase-modulated interference signal and its Hilbert transform or a filtering process [12–18]. The modified versions of the lateral Hilbert transform have been demonstrated to obtain Doppler OCT images [19,20] and optical angiograms [21,22]. However, implementing the lateral Hilbert transform that involves two Fourier transforms requires significantly more computing time.

Therefore, FD-OCT requires high-speed signal-processing techniques to obtain real-time images, a near necessity in clinical applications such as endoscopy and ophthalmology. Most high-speed processing is performed using multicore central processing units (CPUs). By using a parallel computing quad-core CPU, real-time OCT-data processing of an 80 kHz A-line with a 1024-point fast Fourier transform (FFT) becomes possible [23]. However, because one core was used for data acquisition and OCT image display, only three cores remain for data processing. The alternative of adopting two quad-core CPUs or a high-end six-core CPU is an expensive proposition.

Digital signal processing (DSP) hardware has also been used to display OCT images in real time [24–26]. DSP hardware with a single field-programmable gate array (FPGA) integrated circuit and a custom electronics board has demonstrated a display frame rate for processed OCT images (1024 axial pixels× 512 lateral A-scans) of 27 fps in a SD-OCT system [26]. This type of equipment is expensive and must be custom built for FPGA technology.

Recently, one approach to accelerating numerical calculations has been to use a graphic processing unit (GPU) instead of a CPU. A GPU, with its many stream processors, provides highly parallel computing at a low cost, plus there is the advantage of simple programming on the host computer. In optics, GPU techniques have been applied to reconstruct digital holograms [27–29]. Real-time 512 × 512 pixel images are reconstructed from holograms at 24 fps by calculating a Fresnel diffraction integral involving two forward two-dimensional (2D)-FFTs and one inverse 2D-FFT [29]. We have similarly demonstrated a real-time display of processed OCT images using a linear-in-wave number spectrometer and a GPU [30]. The FFT calculation was accelerated by the GPU so that the computing time was 6.1 ms for 2048-point FFT × 1000 lateral A-scan data, and it was much shorter than the 35.8 ms frame-interval time of the interference frame. The computing time on the GPU had a wide margin for the FFT process only in our SD-OCT system. More recently, the real-time resampling processes in standard FD-OCT have been demonstrated using GPU programming [31,32]. The GPU-based processing times achieved a speedup of 15 to 20 times when compared to LabVIEW algorithms on a host computer with eight Intel Xeon E5405 processing cores [32].

In this paper we demonstrate the real-time display of a full-range OCT image with zero-filling interpolation using GPU programming. The computing times for 2048 axial pixels × 1024 lateral A-lines were 26.88 ms using a single GPU and 14.75 ms using dual GPUs, including the zero-filling linear interpolation by increasing the data-array length fourfold, then doing a lateral Hilbert transform, an axial Fourier transform, and a log scaling. With the 15.73 ms frame-grabber data transfer, the use of dual GPUs achieved a real-time OCT image display rate of 27.23 fps using a line-scan 27.9 kHz CCD camera.

2. Experimental Setup

Figure 1 shows a schematic of our SD-OCT system. The output light of a superluminescent diode (SUPERLUM; with center wavelength $\lambda_0 = 840$ nm and spectral bandwidth $\Delta\lambda = 50$ nm) was split into sample and reference arms, with the latter

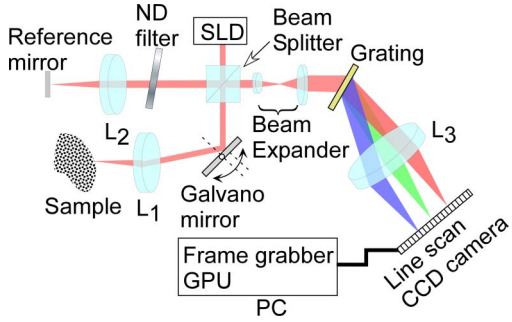

Fig. 1. (Color online) Schematic of spectral-domain optical-coherence tomography: SLD, superluminescent diode; L, achromatic lens; ND filter, neutral density filter.

terminated by a mirror. A probe at the end of the sample arm delivered light to a sample and received backscattered light from within the sample. Achromatic lenses ($f = 35$ mm) were inserted in both arms. The measured lateral resolution was 15.6 μm. The probe beam was scanned at 27.23 Hz using a sawtooth waveform with a 98% duty cycle, which had been modified to reduce mechanical vibrations. We used the beam-spot offset on the scanning mirror to obtain a 6 kHz carrier frequency in the spatial direction. The method has the advantage of not requiring any modulators [14–16]. The light returned from the two interferometer arms was recombined and directed to a diffraction grating (Wasatch Photonics, Volume Phase Holographic Grating, 1200 lines/mm) and then focused on a line-scan CCD camera (e2v Aviiva SM2, 2048 pixels, 14 μm pixel size, 12 bit resolution, line rate $f_{\text{scan}} = 27.9$ kHz) using an achromatic lens ($f = 200$ mm). The camera output was ported to a personal computer (PC) via a low-cost camera-link board (National Instruments, PCIe-1427, 16 bit resolution) having a 200 MB/s transfer rate to the PCI Express x1 interface.

In our system, 2048 × 1024 pixels at 12 bit resolution can be obtained at intervals of 36.70 ms. Because the image size is 3.15 MB, the data transfer to the host computer memory takes $3.15\,(\text{MB})/200\,(\text{MB/s}) = 15.73$ ms via the frame grabber for the PCI Express x1 interface. Therefore, to display a real-time OCT image, the signal processing must execute in less than 20.97 ms.

Signal processing was performed using a graphics card (NVIDIA, GeForce GTX 295) with two GPUs (1296 MHz processor clock, 1998 MHz memory clock, 240 stream processors per GPU, and 896 Mbytes per GPU memory). We used NVIDIA's compute unified device architecture (CUDA) [33], which could be programmed in a C language environment to exploit the processing power of the GPUs. We developed software that included image acquisition, GPU programming, and a graphic user interface environment in Microsoft Visual C++, 2008 Express Edition.

3. Signal Processing of Full-Range OCT with Zero-Filling Interpolation

In SD-OCT, the combined backreflected sample and reference light in an interferometer are detected by a spectrometer together with an array detector, such as a line-scan camera. The depth-encoded spectral interferometric signal can be written as

$$S(\lambda, x) = I_S + I_R + \int 2(I_S I_R)^{1/2} \cos[2\pi/\lambda \cdot z + \phi(x)]\mathrm{d}z, \tag{1}$$

where I_R and I_S are the intensities of the reference and reflected from the sample light at depth z, and ϕ is the phase difference modulated in the lateral direction. Because these spectral data are nonlinear in k-space, they must be resampled to produce a spectrum linear in k prior to taking the Fourier transform. After increasing the data-array size by the zero-filling technique, the nth point of S_k in linear interpolation from λ-space S_λ to k-space S_k can be obtained from

$$S_k[n] = (1 - X_2[n])S_\lambda[X_1[n]] + X_2[n]S_\lambda[X_1[n] + 1], \tag{2}$$

where X_1 and X_2 are the array index and coefficient that can be obtained by calibrating the spectrometer.

The Hilbert transform is performed in the lateral direction to obtain the analytic spectral interferometric signal. This transforms a real-valued signal S_k into a complex-valued signal S_A. The real part of S_A is identical to the input signal, and the imaginary part is a $(-\pi/2)$-phase-shifted version (or the Hilbert transform S_H of S_k). The complex analytic signal in the spatial domain is described as

$$S_A(k, x) = S_k(k, x) - iS_H(k, x). \tag{3}$$

In the frequency domain, the analytic signal was derived from the input signal by suppressing its negative frequency components and multiplying the positive ones by 2. The frequency-domain complex-analytic signal is then written as

$$\mathrm{FT}_{x\to u}[S_A(k, x)] = H(u)\mathrm{FT}_{x\to u}[S(k, x)], \tag{4}$$

where $H(u)$ is the Heaviside step function given by

$$H(u) = \begin{cases} 2 & u > 0 \\ 0 & u \le 0 \end{cases}. \tag{5}$$

Because the reference intensity is constant in the lateral direction, this filtering also acts to remove the reference intensity. As shown in Fig. 2, we also applied the modified step function to reduce the DC components of the sample beam. Finally, an inverse Fourier transform was performed to obtain the full-range OCT image. The log-scaled OCT signal is described as

$$\mathrm{OCT}(z, x) = 10\,\log\{\mathrm{FT}_{k\to z}[S_A(k, x)]\}. \tag{6}$$

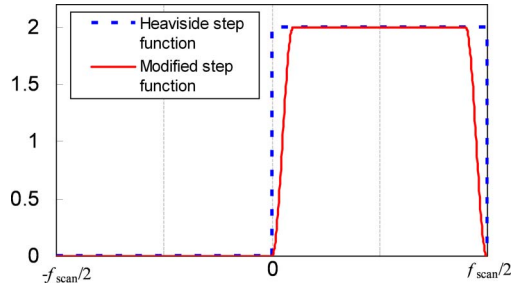

Fig. 2. (Color online) Heaviside step function and modified step function.

4. Results and Discussions

A. Signal Processing Using GPU

Figure 3 shows the flow chart of the signal processing using a GPU. The Fourier transform was carried out using the CUDA FFT operating in 32 bit floating-point (single precision) mode. Initially, the constant values (I_R, X_1, X_2, and H) are transferred to the GPU memory only once. The reference intensity distribution I_R is used to obtain a half-range OCT (i.e., a standard OCT) image. The captured spectral interference image ($N_z = 2048$ axial pixels $\times N_x = 1024$ lateral pixels, 16 bit) is transferred to memory on the GPU. Next, the data type is converted from 16 bit integer to 32 bit floating point and then, if necessary, the DC removal is performed. The real and imaginary parts of the complex data are set to the processed data and zero, respectively.

In the simple linear interpolation, this spectrum is resampled in k-space using the initially stored constants. Because the data-array length is the same as the captured data, M is 1. The zero-filling interpolation is performed with an FFT, zero padded to increase the data-array length fourfold ($M = 4$), inverse Fourier transformed back to the spectral domain, and linear interpolated in k-space.

To obtain a full-range OCT image, an N_x-point FFT is first executed for MN_z axial points after transposing the matrix. Next, the coefficients of the Hilbert transform are multiplied with the Fourier transformed data, followed by an N_x-point inverse FFT being executed for MN_z axial points

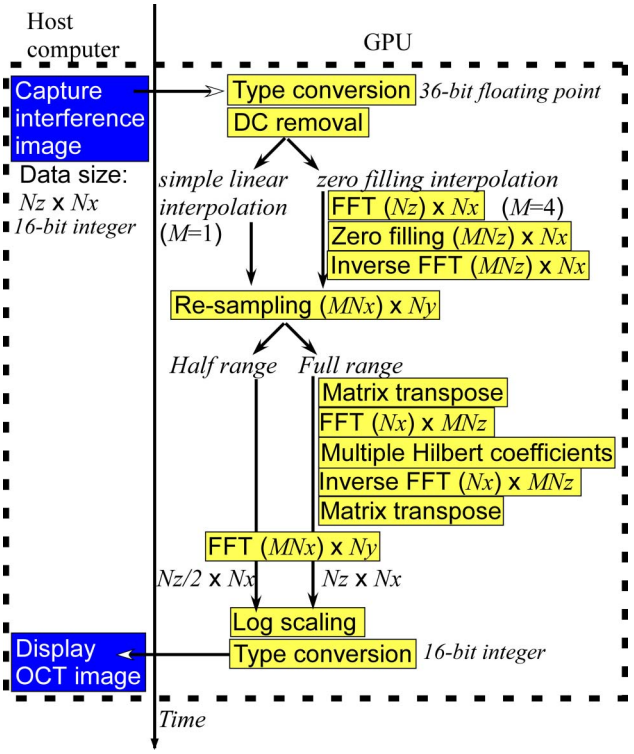

Fig. 3. (Color online) Flow chart of signal processing of OCT image using a GPU.

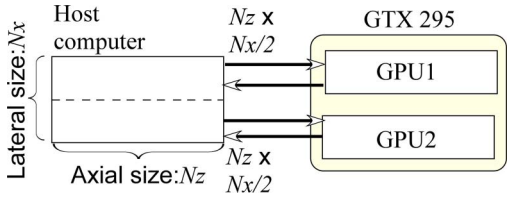

Fig. 4. (Color online) Data flow of dual GPUs processing.

and then another matrix transpose. To obtain depth profiles, the MN_z-point FFT is executed for N_x lateral points. The log-scaling process is then performed to obtain an $N_z \times N_x$ full-range or an $N_z/2 \times N_x$ half-range OCT image. The data are then converted from 32 bit float to 16 bit integer; the results are transferred to the host computer memory and, finally, displayed on the monitor.

Figure 4 shows the GPU computing data flow using dual GPUs. The half data ($N_z \times N_x/2$) in the lateral direction are transferred to each memory on the GPU. In our case, the first 512 A-lines (from the first to 512th) and the last 512 A-lines (from the 512th to 1024th) are transferred to GPU1 and GPU2, respectively. These procedures execute on each GPU and then combine to build an OCT image in the host computer memory. This parallel computing was performed via OpenMP [34].

B. Processing Time on GPU

We measured processing times for the transfers to and from the GPU memory using a single GPU and dual GPUs by executing the timer function on C language (see Fig. 5). Here, these times were the average of 100 times. The procedures A, B, C, and D correspond to the full-range OCT with zero-filling interpolation, the half-range OCT with zero-filling interpolation, the full-range OCT with simple-linear interpolation, and the half-range OCT with simple-linear interpolation, respectively. The procedure A took the processing time of 26.88 ms by calculating a single GPU, and cannnot display the OCT images in real time. To achieve a real-time display with

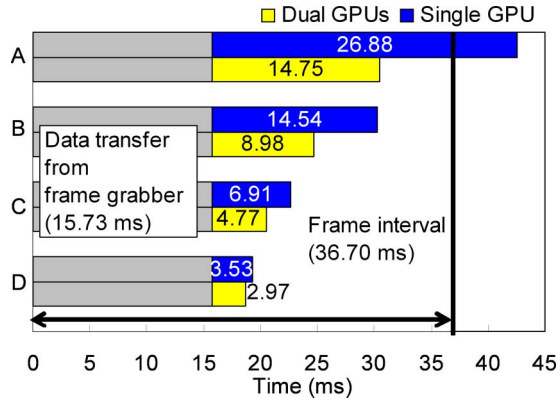

Fig. 5. (Color online) Processing times using single GPU and dual GPUs. A: full-range OCT with zero-filling interpolation. B: half-range OCT with zero-filling interpolation. C: full-range OCT with simple linear interpolation. D: half-range OCT with simple linear interpolation.

procedure A and a single GPU, the data transfer needed to be reduced using a high-speed frame grabber with the PCI Express x4 interface. If we choose a high-speed camera link board (National Instruments, PCIe-1429), which has 680 MB/s transfer rates, the data-transfer time would be reduced by about $3.15\,(\mathrm{MB})/680\,(\mathrm{MB/s}) = 4.63\,\mathrm{ms}$, yielding a resultant total time of 31.51 ms, which is also shorter than the frame-interval time. Furthermore, we estimated a total 7.6 ms time for procedure D (i.e., the standard OCT imaging) by combining a high-speed frame grabber with a 4.63 ms transfer time with dual GPUs having processing times of 2.97 ms. This time corresponds to 131.6 fps for 2048 axial × 1024 lateral points by capturing 134.7 k A-scans/s.

Generally, the signal processing with dual GPUs was faster than with a single GPU. However, the difference was small for procedure D because the data transfer between the GPU and the host computer dominates when an easy processing task executes on the GPU. Although the selected graphics card has two GPUs, it fits in a single PCI Express slot so that both GPUs use a single bus. Two graphics cards, fitting in two slots, would reduce the data-transfer time.

C. *In Vivo* OCT Imaging

First, we measured the SNR of our OCT system with a probing power of 5.0 mW and an integration time of 34 μs. Here, the sample used was a plane mirror with the attenuation of 50 dB. Figures 6(a) and 6(b) show the SNR falloff at zero-filling interpolation and simple linear interpolation, respectively. The measured full-depth range was 6.78 mm (3.39 mm × 2). The SNR around the zero-delay was 102 dB with an axial resolution of 9 μm in air with a 6 dB falloff at 1 mm.

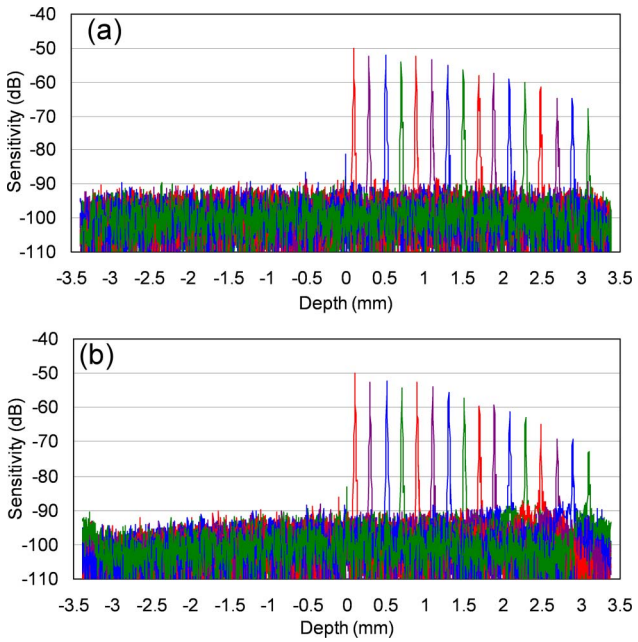

Fig. 6. (Color online) SNR fall off (a) zero-filling interpolation (b) simple linear interpolation.

From this comparison, the zero-filling technique improved to the SNR at greater depth. GPU-based cubic spline interpolation was effective to improve image quality [32]. Because the zero-filling interpolation requires much processing time compared to cubic spline interpolation, the GPU computing is helpful to achieve real-time display. The more detailed comparisons of GPU-based zero-filling and cubic spline interpolation will be performed in our future work.

Next, we measured the OCT images of a human-nail-fold region around the zero delay. By using dual GPUs, real-time, full-range OCT imaging was displayed at 27.23 fps. Figure 7(a) shows the full-range $5.0 \times 6.78\,\mathrm{mm}^2$ (lateral × axial) OCT image; for comparison, Fig. 7(b) shows the standard OCT image. In Fig. 7(b), as we performed the DC removal using the reference beam intensity, the DC component of the sample beam still resides at zero delay. Therefore, the modified step function was effective in removing the DC components of the sample and reference beams. Figure 8 (Media 1) shows the captured movie of our graphic user interface in measuring a finger pad. Here, the size of the OCT image was reduced to 1024 × 1024 pixels to display the monitor (1920× 1080 pixel resolution). In full-range FD-OCT, a target needs to be relatively static to remove the complex conjugate artifact. This artifact appears while the phase delay caused by axial motion of a target is comparable to the intrinsic delay by offsetting the galvo scanning mirror. If the axial motion speed is 400 μm/s, this motion is generated about 6 kHz in frequency shift in the lateral direction and cancels the 6 kHz carrier frequency generated by the scanning mirror. Since the axial motion of target is a big concern to determine whether the complex conjugate artifact can be removed successfully, the GPU-based real-time

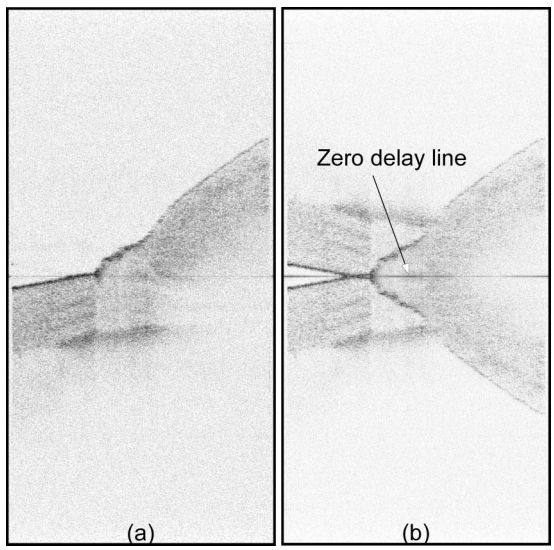

Fig. 7. (a) Full-range OCT image, (b) standard OCT image of a human-nail-fold region. Imaging range: $5.0 \times 6.78\,\mathrm{mm}^2$ (lateral × axial).

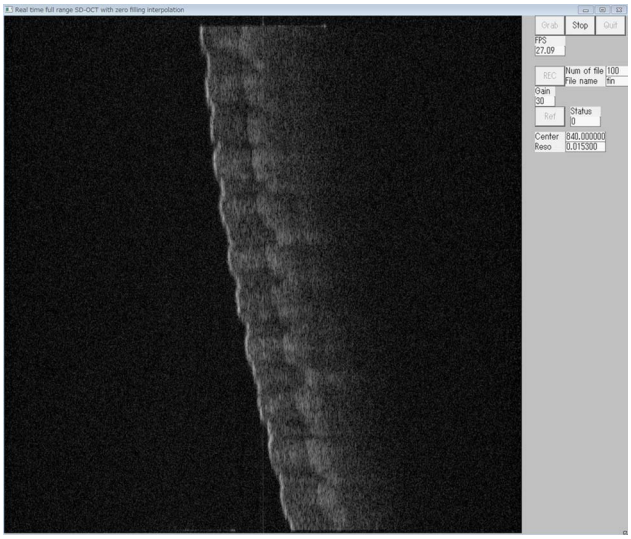

Fig. 8. (Color online) (Media 1) Captured graphic user interface in measuring a finger pad.

processing is useful to monitor the success or not in the processed full-range OCT images.

5. Conclusion

We demonstrated full-range, real-time, 2048 axial × 1024 lateral pixel SD-OCT images using a zero-filling technique with a low-cost GPU. With a 15.73 ms data-transfer time for the low-cost frame grabber and a GPU processing time of 14.75 ms, the total time was shorter than the frame-interval time of 36.70 ms using a 27.9 kHz line-scan CCD camera. By adding the graphics board with a CUDA-enabled GPU to the computer, this technique can easily be applied to swept source OCT systems. Since the GPUs are more cost-effective in displaying real-time FD-OCT images than techniques using, for example, high-end CPUs and FPGAs, this technique is very promising for a variety of applications.

This study was partially supported by Grant-in-Aid for Scientific Research (20700375) in the Japan Society for the Promotion of Science (JSPS) and the Industrial Technology Research Grant Program in 2005 from the New Energy and Industrial Technology Development Organization (NEDO) of Japan.

References

1. D. Huang, E. A. Swanson, C. P. Lin, J. S. Schuman, W. G. Stinson, W. Chang, M. R. Hee, T. Flotte, K. Gregory, C. A. Puliafito, and J. G. Fujimoto, "Optical coherence tomography," Science **254**, 1178–1181 (1991).
2. A. F. Fercher, C. K. Hitzenberger, G. Kamp, and S. Y. El-Zaiat, "Measurement of intraocular distances by backscattering spectral interferometry," Opt. Commun. **117**, 43–48 (1995).
3. G. Häusler and M. W. Lindner, ""Coherence Radar" and "Spectral Radar"—New Tools for Dermatological Diagnosis," J Biomed. Opt. **3**, 21–31 (1998).
4. S. Yun, G. Tearney, J. de Boer, N. Iftimia, and B. Bouma, "High-speed optical frequency-domain imaging," Opt. Express **11**, 2953–2963 (2003).
5. N. Nassif, B. Cense, B. H. Park, S. H. Yun, T. C. Chen, B. E. Bouma, G. J. Tearney, and J. F. de Boer, "*In vivo* human retinal imaging by ultrahigh-speed spectral domain optical coherence tomography," Opt. Lett. **29**, 480–482 (2004).
6. R. A. Leitgeb, C. K. Hitzenberger, and A. F. Fercher, "Performance of Fourier domain vs. time domain optical coherence tomography," Opt. Express **11**, 889–894 (2003).
7. R. Huber, D. C. Adler, and J. G. Fujimoto, "Buffered Fourier domain mode locking: unidirectional swept laser sources for optical coherence tomography imaging at 370,000 lines/s," Opt. Lett. **31**, 2975–2977 (2006).
8. B. Potsaid, I. Gorczynska, V. J. Srinivasan, Y. Chen, J. Jiang, A. Cable, and J. G. Fujimoto, "Ultrahigh speed Spectral/Fourier domain OCT ophthalmic imaging at 70,000 to 312,500 axial scans per second," Opt. Express **16**, 15149–15169 (2008).
9. C. Dorrer, N. Belabas, J.-P. Likforman, and M. Joffre, "Spectral resolution and sampling issues in Fourier transform spectral interferometry," J. Opt. Soc. Am. B **17**, 1795–1802 (2000).
10. N. A. Nassif, B. Cense, B. H. Park, M. C. Pierce, S. H. Yun, B. Bouma, and G. Tearney, "In vivo high-resolution video-rate spectral-domain optical coherence tomography of the human retina and optic nerve," Opt. Express **12**, 367–376 (2004).
11. Y. Yasuno, V. D. Madjarova, S. Makita, M. Akiba, A. Morosawa, C. Chong, T. Sakai, K.-P. Chan, M. Itoh, and T. Yatagai, "Three-dimensional and high-speed swept-source optical coherence tomography for in vivo investigation of human anterior eye segments," Opt. Express **13**, 10652–10664 (2005).
12. Y. Yasuno, S. Makita, T. Endo, G. Aoki, M. Itoh, and T. Yatagai, "Simultaneous B-M-mode scanning method for real-time full-range Fourier domain optical coherence tomography," Appl. Opt. **45**, 1861–1865 (2006).
13. R. K. Wang, "In vivo full range complex Fourier domain optical coherence tomography," Appl. Phys. Lett. **90**, 054103 (2007).
14. B. Baumann, M. Pircher, E. Götzinger, and C. K. Hitzenberger, "Full range complex spectral domain optical coherence tomography without additional phase shifters," Opt. Express **15**, 13375–13387 (2007).
15. R. A. Leitgeb, R. Michaely, T. Lasser, and S. C.Sekhar, "Complex ambiguity-free Fourier domain optical coherence tomography through transverse scanning," Opt. Lett. **32**, 3453–3455 (2007).
16. L. An and R. K. Wang, "Use of a scanner to modulate spatial interferograms for *in vivo* full-range Fourier-domain optical coherence tomography," Opt. Lett. **32**, 3423–3425 (2007).
17. S. Vergnole, G. Lamouche, and M. L. Dufour, "Artifact removal in Fourier-domain optical coherence tomography with a piezoelectric fiber stretcher," Opt. Lett. **33**, 732–734 (2008).
18. S. Makita, T. Fabritius, and Y. Yasuno, "Full-range, high-speed, high-resolution 1 μm spectral-domain optical coherence tomography using BM-scan for volumetric imaging of the human posterior eye," Opt. Express **16**, 8406–8420 (2008).
19. Y. K. Tao, A. M. Davis, and J. A. Izatt, "Single-pass volumetric bidirectional blood flow imaging spectral domain optical coherence tomography using a modified Hilbert transform," Opt. Express **16**, 12350–12361 (2008).
20. Y. K. Tao, K. M. Kennedy, and J. A. Izatt, "Velocity-resolved 3D retinal microvessel imaging using single-pass flow imaging spectral domain optical coherence tomography," Opt. Express **17**, 4177–4188 (2009).
21. R. K. Wang, S. L. Jacques, Z. Ma, S. Hurst, S. R. Hanson, and A. Gruber, "Three-dimensional optical angiography," Opt. Express **15**, 4083–4097 (2007).
22. L. An and R. K. K. Wang, "In vivo volumetric imaging of vascular perfusion within human retina and choroids with optical micro-angiography," Opt. Express **16**, 11438–11452 (2008).

23. G. Liu, J. Zhang, L. Yu, T. Xie, and Z. Chen, "Real-time polarization-sensitive optical coherence tomography data processing with parallel computing," Appl. Opt. **48**, 6365–6370 (2009).
24. S. Yan, D. Piao, Y. Chen, and Q. Zhu, "Digital signal processor-based real-time optical Doppler tomography system," J Biomed. Opt. **9**, 454–463 (2004).
25. J. Su, J. Zhang, L. Yu, H. G. Colt, M. Brenner, and Z. Chen, "Real-time swept source optical coherence tomography imaging of the human airway using a microelectromechanical system endoscope and digital signal processor," J. Biomed. Opt. **13**, 030506 (2008).
26. T. E. Ustun, N. V. Iftimia, R. D. Ferguson, and D. X. Hammer, "Real-time processing for Fourier domain optical coherence tomography using a field programmable gate array," Rev. Sci. Instrum. **79**, 114301 (2008).
27. N. Masuda, T. Ito, T. Tanaka, A. Shiraki, and T. Sugie, "Computer generated holography using a graphics processing unit," Opt. Express **14**, 587–592 (2006).
28. L. Ahrenberg, P. Benzie, M. Magnor, and J. Watson, "Computer generated holography using parallel commodity graphics hardware," Opt. Express **14**, 7636–7641 (2006).
29. T. Shimobaba, Y. Sato, J. Miura, M. Takenouchi, and T. Ito, "Real-time digital holographic microscopy using the graphic processing unit," Opt. Express **16**, 11776–11781 (2008).
30. Y. Watanabe and T. Itagaki, "Real-time display on Fourier domain optical coherence tomography system using a graphics processing unit," J Biomed. Opt. **14**, 060506 (2009).
31. K. Zhang and J. U. Kang, "Real-time 4D signal processing and visualization using graphics processing unit on a regular nonlinear-k Fourier-domain OCT system," Opt. Express **18**, 11772–11784 (2010).
32. S. Van der Jeught, A. Bradu, and A. Gh. Podoleanu, "Real-time resampling in Fourier domain optical coherence tomography using a graphics processing unit," J. Biomed. Opt. **15**, 030511 (2010).
33. NVIDIA CUDA Zone, http://www.nvidia.com/object/cuda_home.htm.
34. OpenMPArchitecture Review Board, "The OpenMPAPI specification for parallel programming," http://www.openmp.org/.